Formation and ripening of alginate-like exopolymer gel layers during and after membrane filtration

Pfaff, N. M.; Kleijn, J. Mieke; van Loosdrecht, Mark C.M.; Kemperman, Antoine J.B.

DOI
10.1016/j.watres.2021.116959

Publication date
2021

Document Version
Final published version

Published in
Water Research

Water Research 195 (2021) 116959

Contents lists available at ScienceDirect

Water Research

journal homepage: www.elsevier.com/locate/watres

Formation and ripening of alginate-like exopolymer gel layers during and after membrane filtration

N.-M. Pfaff[a,c,*], J. Mieke Kleijn[b], Mark C.M. van Loosdrecht[a], Antoine J.B. Kemperman[c,d]

[a] TNW Applied Sciences, TU Delft, Van der Maasweg 9, 2629 HZ Delft, The Netherlands
[b] Physical Chemistry and Soft Matter, Wageningen University, Helix, 124, Stippenweg 4, 6708 WE Wageningen, The Netherlands
[c] Wetsus, European Center of Excellence for Sustainable Water Technology, Oostergoweg 9, 8911 MA Leeuwarden, The Netherlands
[d] Membrane Science and Technology cluster, Faculty of Science and Technology, Mesa+ Institute for Nanotechnology, University of Twente, P.O. Box 217, 7500 AE Enschede, The Netherlands

ARTICLE INFO

Article history:
Received 21 October 2020
Revised 17 February 2021
Accepted 19 February 2021
Available online 23 February 2021

Keywords:
Extracellular polymeric substances
Calcium-binding
Hydrogel
Donnan potential
Biofilm

ABSTRACT

The properties of biofilm EPS are determined by the multiple interactions between its constituents and the surrounding environment. Because of the high complexity of biofilm EPS, its constituents' characterisation is still far from thorough, and identification of these interactions cannot be done yet. Therefore, we use gels of bacterial alginate-like exopolysaccharides (ALEs) as a model component for biofilm EPS in this work. These gels have been examined for their cohesive properties as a function of $CaCl_2$ and KCl concentration. Hereto, ALE gel layers were formed on membranes by dead-end filtration of ALE solutions. Accumulation of the cations Ca^{2+} and K^+ in the gels could be well predicted from a Donnan equilibrium model based on the fixed negative charges in the ALE. This suggests that there is no specific binding of Ca^{2+} to the ALE and that on the time scale of the experiments, the Ca^{2+} ions can distribute freely over the gel and the surrounding solution. The concentration of fixed negative charges in the ALE was estimated around 1 mmol/g VSS (volatile suspended solids, organic mass) from the Donnan equilibrium. Moreover, an accumulation of H^+ was predicted. Gels with more $CaCl_2$ in the supernatant were more compact and bore a higher osmotic pressure than those with less $CaCl_2$, revealing the role of Ca^{2+} ions in the network crosslinking. It is hypothesised that this mechanism later transitions into a rearrangement of the ALE molecules, which eventually leads to a fibrous network structure with large voids.

1. Introduction

The integrity of biofilms, also when exposed to harsh cleaning attempts, has been assigned to their polymeric matrix (Seviour et al., 2019). The matrix is often also referred to as extracellular polymeric substances (EPS). It has been found to consist of a complex mixture of biopolymers, such as polysaccharides and proteins, complemented by lipids, humic substances and eDNA. The EPS matrix has been described as a physically crosslinked hydrogel (Seviour et al., 2009), in reference to its ability to incorporate up to 99 % water while providing a lasting polymeric network structure. In contrast to chemically crosslinked networks, the crosslinks in physically linked networks are provided by non-covalent interactions. These are particularly electrostatic interactions, hydrophobic interactions, H-bonding and van-der-Waals forces, and entanglements. They are reversible. Essential parameters of hydrogels are their degree of crosslinking, determined for example by the number of charges on the polymers, their interaction with counter-ions, and their hydrophilicity (Ganji et al., 2010). The interplay of forces following from these parameters determines the state of swelling of the hydrogel under steady-state conditions (Bajpai, 2001) and their potential for water storage.

The swelling state has been identified as a crucial parameter with regards to adhesion, mechanical strength, permeability and degradation behaviour of hydrogels (Davidovich-Pinhas and Bianco-Peled, 2010). These properties also have been used to characterise biofilms. Adhesion and mechanical strength have been correlated with fouling potential (Li and Elimelech, 2004) and success of cleaning strategies (Safari et al., 2015). The increase of hydraulic resistance resulting from biofouling on membranes has been labelled as a huge impediment for membrane filtration systems (Flemming, 2020). It strikes, therefore, that the number of studies about swelling of biofilms and EPS is minor so far. Changes

* Corresponding author: Hauffstr. 18, 34125 Kassel, Germany
E-mail addresses: n.dietrich@tudelft.nl, n.m.pfaff@gmail.com, natascha.m.pfaff@gmail.com (N.-M. Pfaff), M.C.M.vanLoosdrecht@tudelft.nl (M.C.M. van Loosdrecht).

https://doi.org/10.1016/j.watres.2021.116959

in swelling behaviour of EPS have been described as a function of pH for EPS extracted from activated sludge as well as for EPS extracted from different bacterial cultures (Radchenkova et al., 2018).

To understand the molecular interactions and allocate functions to molecules or functional groups, simplification of the EPS matrix is necessary. A promising model are alginate-like exopolymers (ALE), which are identified as crucial structural EPS components (Lin et al., 2010). Like the well-characterised and often used alginate extracted from brown algae, gel-formation with Ca^{2+} ions has been observed (Felz et al., 2020a). A full chemical analysis of ALE is still pending (Seviour et al., 2019). Still, it was used in this work as a simple approximation for the complexity of biofilm EPS. Ca^{2+} availability has been identified as an essential factor for biofilm stability (Körstgens et al., 2001) and has been shown to induce crosslinking of ALE. Therefore, the effect of variations in its concentration was investigated in this study as well. Based on the impact of monovalent ions (Wang and Spencer, 1998) and ionic strength (van den Brink et al., 2009) on the structurally similar Ca-alginate gels, KCl was chosen as a second ionic component. Ca-ALE gel layers were produced on membranes in dead-end filtration mode. Although usually membrane filtration operates in cross-flow mode, dead-end filtration was chosen since this method was found to produce sufficiently thick films to investigate using OCT, and to focus on the cohesive forces of the bulk ALE gel. From the swelling behaviour of the obtained thick ALE layers, conclusions were drawn on the binding behaviour of ALE in the network-formation of EPS, with a particular focus on the interaction with Ca^{2+}. The final composition (density, ions) and cake layer resistances of the gel layers were correlated with the availability of Ca^{2+} and K^{+} and the solutions' ionic strength. Furthermore, the gel layers' ripening was observed for 12 days. The results were analysed based on the Donnan equilibrium.

2. Materials and methods

ALE gel layers cross-linked with Ca^{2+} were produced by pressure driven dead-end filtration in the presence of $CaCl_2$ and KCl. Their swelling behaviour was observed for up to two weeks. Eventually, their composition was determined and interpreted.

2.1. ALE extraction and characterisation

The alginate-like exopolymers used in this study were extracted from Nereda® sludge, collected from the wastewater treatment plant in Garmerwolde, the Netherlands (described by Pronk et al., 2015). A combination of added Na_2CO_3, sonication, and high temperature was used for extraction, following procedures defined by Felz et al., 2016.

Granules were collected by decanting. About 150 g of wet granules (20 g dry weight) were mixed with 1 L demineralised water and 10 g Na_2CO_3 (VWR, The Netherlands), resulting in a 1 % (m/v) carbonate solution. The mixture was homogenised with a Branson Sonifier 250 for 5 min at 70 % (of 200 W) in pulsed mode. Overheating of the solution was prevented using an ice bath. The mixture was then heated to 80 °C and vigorously stirred for 30 min. After centrifugation (Allegra X-12R Centrifuge, Beckman Coulter, 20 min, 3750 rpm), the supernatant was acidified with 1 M hydrochloric acid (Merck Millipore, Germany) to a final pH 2 - 2.5. The solution was centrifuged again (20 min, 3750 rpm), and the pellet was stored at -80 °C until further use. It is hereafter referred to as ALE.

After extraction, the ALE was tested for its gel-forming ability with $CaCl_2$ (Felz et al., 2016). The acidic pellet was dissolved and neutralised with 1 M NaOH (Merck Millipore, Germany). Drops of the neutral ALE were dripped into a 2.5 % (m/v) $CaCl_2$ solution. Gelling was considered successful if gel beads could be observed in the solution.

The dry and organic masses of the ALE extract were determined in triplicate. Samples were weighed into dry porcelain crucibles (m_{sample}) and heated to 105°C for 24h. Afterwards, the dry sample weight (total suspended solids, *TSS*) was determined. After subsequent heating to 550°C for 2 hours, the ash's mass was measured (m_{ash}). The organic mass (*VSS*) was defined as the difference between *TSS* and m_{ash}.

2.2. Experiments

Experiments were performed with two different ALE concentrations. Gel layers with 60 mg/L and 45 mM ionic strength were observed for structural changes with OCT over five days. Duplets of layers with 1 mM $CaCl_2$/42 mM KCl, 3 mM $CaCl_2$/36 mM KCl and 15 mM $CaCl_2$ were used. Due to their structural inhomogeneity, the latter gels were not further analysed.

Gel layers with 120 mg/L ALE stayed structurally uniform over the whole observation period and were used to calculate ion distributions. An overview of their ionic combinations is given in Table 1. For each ion combination, three feed solutions were produced, each split over two membranes. While two of the gel layers were directly analysed for their composition, quadruplets of each combination were observed for two weeks concerning their swelling behaviour (storage at 4°C to retard microbial growth).

A further test on the influence of the supernatant composition on the swelling state was done with the underlined combinations in Table 1. Three gel layers were prepared with 3 mM $CaCl_2$ and 6 mM KCl. One sample (F) was directly transferred to a storage solution with 12 mM $CaCl_2$ and 6 mM KCl, the other two (a blank and the test gel layer "L") were observed for two days in the corresponding storage solution. After two days, sample L was also transferred to a storage solution with 12 mM $CaCl_2$ and 6 mM KCl, and the thicknesses of all gel layers were recorded for another five days.

Especially in case of the divalent Ca^{2+} ion, a significant difference between the nominal concentration c_i and the effective activity a_i was expected. Applying an extended Debye-Hückel equation that considers ion sizes (Kielland, 1937), the activity coefficients γ_i were determined as a function of the ionic strength I, the valence z_i and the hydrated radius r_i of the ions.

$$\log \gamma_i = \frac{-B \cdot z_i^2 \cdot \sqrt{I}}{1 + r_i \cdot C \cdot \sqrt{I}} \quad (1)$$

In water at 25°C, the values for B and C are $B = 0.51\ M^{-0.5}$ and $C = 3.3\ M^{-0.5}nm^{-1}$ (Hamer and Wu, 1972). The hydrated radii for the relevant ions were taken as 0.3 nm for K^{+} and Cl^{-}, 0.6 nm for Ca^{2+}, and 0.9 nm for H^{+} (Kielland, 1937). The activity coefficients calculated for the solutions of Table 1 can be found in the supporting information (SI), Tables F.

2.3. Model gel layer production

ALE cake layers were prepared by pressure-driven dead-end filtration of feed solutions through ultrafiltration membranes (UP150, polyethersulfone (PES), 150 kDa cut-off, Microdyn Nadir, Wiesbaden, Germany). The compositions of the various feed solutions applied are specified in section 2.2.

For a total volume of 2 L feed solution, the frozen ALE was neutralised with 0.1 M NaOH (Merck Millipore, Germany) and dissolved in 1 L demineralised water by stirring and heating to 40 °C for 1 hour. $CaCl_2 \bullet 2H_2O$ (VWR, the Netherlands) and KCl (VWR, Belgium) were dissolved in 500 mL demineralised water. Both solutions were combined slowly and under stirring, and the mixture

Table 1
Overview of ionic compositions of gel layers. The numbers indicate the ionic strength of the feed solutions. The underlined combinations were subsequently used for testing the reversibility of swelling.

$CaCl_2$ [mM] → KCl [mM] ↓	0	1	3	6	8	12	14
24	24 mM	-	-	42 mM	-	-	-
15	-	-	24 mM	33 mM	-	-	-
6	6 mM	-	15 mM	24 mM	30 mM	42 mM	-
0	-	3 mM	9 mM	18 mM	24 mM	-	42 mM

was filled up to 2 L with demineralised water. The ionic composition was checked with ion chromatography (IC, Metrohm Compact IC 761). 500 mL of storage solutions were prepared for each experiment, with the corresponding composition of $CaCl_2$ and KCl.

The membranes were cut into circles with a diameter of 7.5 cm and immersed in demineralised water for 1 hour. They were mounted at the bottom of 450 mL stainless steel dead-end filtration cells. For the filtration, two cells were connected in parallel to a 10 L pressure vessel that contained the feed solution.

2.3.1. Filtration and cake layer resistance

During filtrations, the feed pressure was set to 1 ± 0.1 bar. The actual pressure (p_a) was recorded alongside the mass of the filtered solution (m_f). To allow uniform gel layer formation, no stirring was applied in the cells. All filtrations were performed at room temperature, 23.9 ± 0.7°C. Initially, the clean water flux was determined for all membranes by filtration of 750 mL of demineralised water at 1 bar. Then, 2 L of the ALE feed solution were added to the pressure vessel and filtered through the two membranes, until 600 mL were filtered through each cell. Filtration took between 18 and 20 hours. The membranes with the model gel layers were removed and stored at 4°C in Petri dishes submerged in the corresponding storage solutions. Between experiments, the cells and tubing were cleaned with 1 % NaOCl and rinsed with demineralised water. The density of water was approximated as $\rho_{H2O} = 1$ g/mL for the course of the experiments, in order to translate the logged data of filtered mass of water m_f at time t to the filtered volume of water V_f.

The transmembrane pressure (TMP) was approximated with the logged applied pressure p_a. The total resistance of the filtration R_f was calculated from p_a and the flux J, using the dynamic viscosity of water at 25°C, 0.89 mPa•s (Nagashima, 1977) for η_{H2O}:

$$R_f(t) = \frac{p_a}{\eta_{H2O} \cdot J(t)} \tag{2}$$

Subtraction of the membrane resistance (calculated from clean water flux) from the total resistance provided the cake layer resistance, R_{cl}.

To characterise the gel layers, the average cake layer resistance over the last hour prior to termination of the filtration was considered. In combination with the organic mass *VSS* per active membrane area A_m (38.5 cm^2), the specific cake resistance α_m was calculated.

2.4. Observation and analysis of the model gel layers

A Ganymede SD-OCT (ThorLabs, Dachau, Germany) was used in combination with the ThorImage® Software to obtain information on each sample's structure and thickness (h). Because the gel layers consisted for more than 90 % of water, the refractive index of water at 25°C of 1.33 was used. Gel layer thicknesses were observed over up to two weeks. The gel layers were also visually inspected for accumulation of bacteria using an Olympus BX40 with a 40x magnification objective.

After the observation period, excess water was removed from the gel layers by gently tapping it off the perpendicular membrane onto a paper towel. The membrane was put on the paper for 10 s. Next, the ALE gel layers were scratched from the membranes. Their *TSS* and *VSS* were determined according to the procedure described in section 2.1. Considering these amounts stable over the observation period, this data was used to calculate the specific cake resistance α_m as well as the organic mass density ρ_{VSS}, the latter with the observed thickness as changing variable. The ash remaining after *TSS* determination was dissolved in 69 % HNO_3 (VWR, France), heating up in a microwave oven (Ethos EASY Advanced Microwave Digestion System, Milestone, Sorisole, Italy) with 1500 mW to 200°C within 15 min, and 200°C for another 15 min. The amounts of Ca^{2+} and K^+ in the gel layers (m_{ion}) were determined using inductively coupled plasma optical emission spectroscopy (ICP-OES, Perkin Elmer, type Optima 5300 DV). The molar concentration was calculated for the different ions in reference to the original ALE gel layer volume.

2.5. Electro-chemical interpretation

For the interpretation of the results, the system is considered as two compartments: the gel layer (compartment 1) and the supernatant (compartment 2) (Fig. 1). The gel is fully penetrable for water and all ions contained in the system (Ca^{2+}, K^+, Cl^-, H^+, OH^-). In addition, the gel layer is considered to contain fixed negative charges, including carboxylic acids and sulfated glycosaminoglycans-like polymers (Felz et al., 2020b).

2.5.1. Electroneutrality

Electroneutrality demands that within each compartment, the charges are balanced.

$$\sum_i z_i \cdot c_{i,2} = 0. \tag{3}$$

$$\sum_i z_i \cdot c_{i,1} - Z = 0 \tag{4}$$

i are the ions specified above, Z is the concentration of fixed negative charges in the gel. In the experiments, the ionic composition in the supernatant was considered controlled and constant due to its substantial volumetric excess compared to the gel layers. The concentrations assumed are, therefore, those shown in Table 1, completed with a negligible concentration of 10^{-4} mM for both H^+ and OH^- (pH 7).

2.5.2. Donnan equilibrium

The Donnan potential describes the electrical potential difference between two compartments due to the uneven distribution of ions as a result of the existence of fixed charges in one of them (here in the ALE). Following from the Nernst equation, it can be calculated as follows

$$E_{Donnan} = \Psi_1 - \Psi_2 = \frac{RT}{z_i \cdot F} \cdot \ln\left(\frac{a_{i,2}}{a_{i,1}}\right) \tag{5}$$

As before, compartment 1 represents the gel phase and 2 stands for the solution. Ψ_1 and Ψ_2 are the respective electrical potentials,

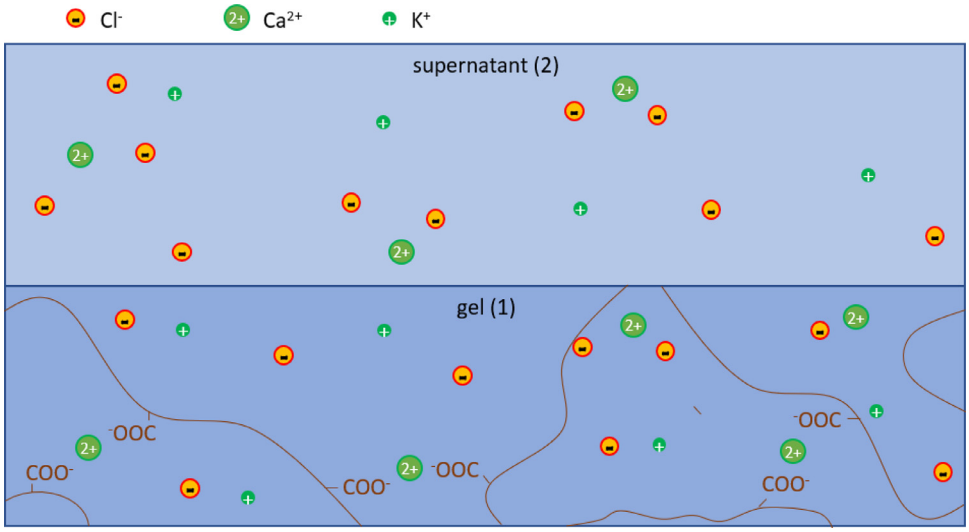

Fig. 1. Schematic display of the two phases in the system: the ALE gel (1) and the supernatant (2). The ions need to balance the fixed negative charges on the ALE polymers.

$a_{i,1}$ and $a_{i,2}$ the activities of ion i in the two compartments, z_i is the valency of the ion, R the gas constant, T the absolute temperature, and F the Faraday constant.

Assuming that there are no specific interactions, the Donnan potential applies to all ions in the system. Equating Eq. 5 for different ions $i = j$ and $i = k$ gives:

$$\left(\frac{a_{j,2}}{a_{j,1}}\right)^{\frac{1}{z_j}} = \left(\frac{a_{k,2}}{a_{k,1\}}}\right)^{\frac{1}{z_k}}. \quad (6)$$

Eq. 6 enables calculating the distribution of a non-quantified ion (like H^+) from the determined distribution of another ion (like Ca^{2+}).

2.5.3. Osmotic pressure

As a consequence of fixed negative charges (as found in the ALE), an uneven ion distribution between gel and supernatant can be established, as described above. This causes an osmotic pressure difference between the gel layers and the supernatant. The osmotic pressure Π in each of the compartments can be calculated from the ionic concentrations using the van 't Hoff equation:

$$\Pi = RT \cdot \sum_i c_i \quad (7)$$

In equilibrium, the gel network withstands the osmotic pressure difference between the gel layer and the supernatant. Therefore, this difference can indicate the strength of the network.

3. Results

3.1. Cake layer resistance

The development of cake layer resistance during filtration is shown in Fig. 2 for a representative experiment (6 mM $CaCl_2$/6 mM KCl). For all experiments executed with $CaCl_2$, similar graphs were obtained. Such shape of the resistance development is common for fouling experiments (Listiarini et al., 2009). The slight concave curvature suggests that the cake layers in this work were compressed during formation (Roorda and van der Graaf, 2001).

The specific cake layer resistance α_m was calculated using the VSS determined directly after filtration. The results are shown in the bubble chart of Fig. 3. Differences between the tested ionic compositions were small. Only with increasing $CaCl_2$ content, a slight increase in the specific cake layer resistance was observed. A systematic effect of KCl was not found.

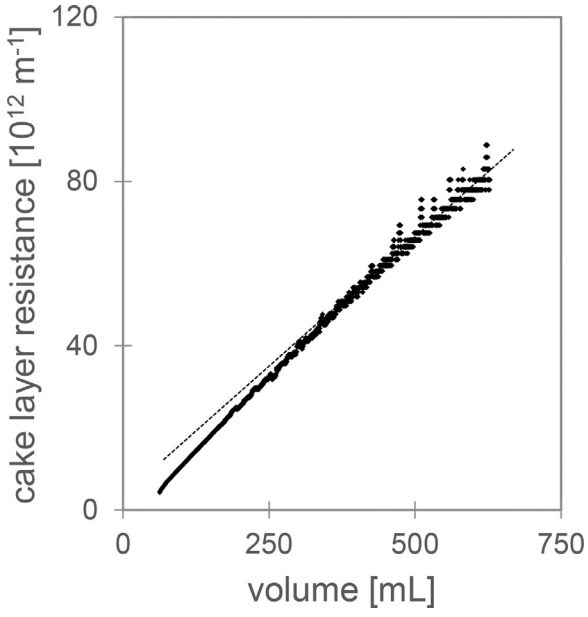

Fig. 2. Development of cake layer resistance throughout filtration, including a trend line for the data above 400 mL. Data is shown for 120 mg/mL ALE, 6 mM $CaCl_2$/6 mM KCl. Data points indicate the averaged resistance over 10 min.

3.2. Composition

3.2.1. Swelling behaviour after preparation

Comparing gel layers analysed directly after production with those examined after 12 days showed no significant differences in VSS content. No microbial growth was observed on the 12 days old gel layers. The amount of ALE was considered constant during the observation period.

It was expected that after the filtration, the gel layers would adjust to the removal of the applied pressure by swelling and eventually reach an equilibrium thickness. This hydrogel-like behaviour has been observed for alginate gel layers under similar conditions (Davidovich-Pinhas and Bianco-Peled, 2010). The equilibration took a long time, though (see Fig. 4). In a prolonged observation period, pores appeared in some gels, as revealed by OCT, which will be discussed in section 3.4. For all gel layers, an initially fast increase in thickness was observed, followed by a period of slower

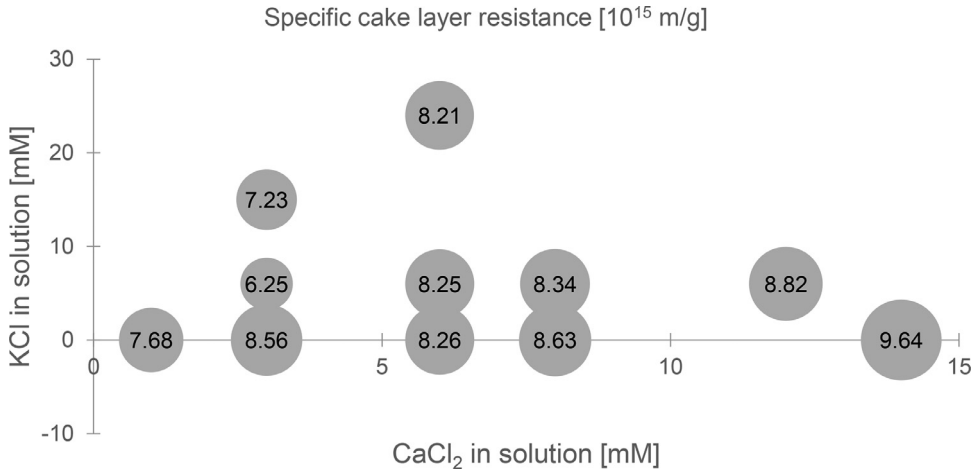

Fig. 3. Bubble chart of the final specific cake layer resistance [10^{15} m/kg] of the ALE gel layers as a function of $CaCl_2$ and KCl concentrations of the solution. The bubble diameter indicates the specific cake layer resistance. Complete data, including standard deviations, are in the SI, Table E.

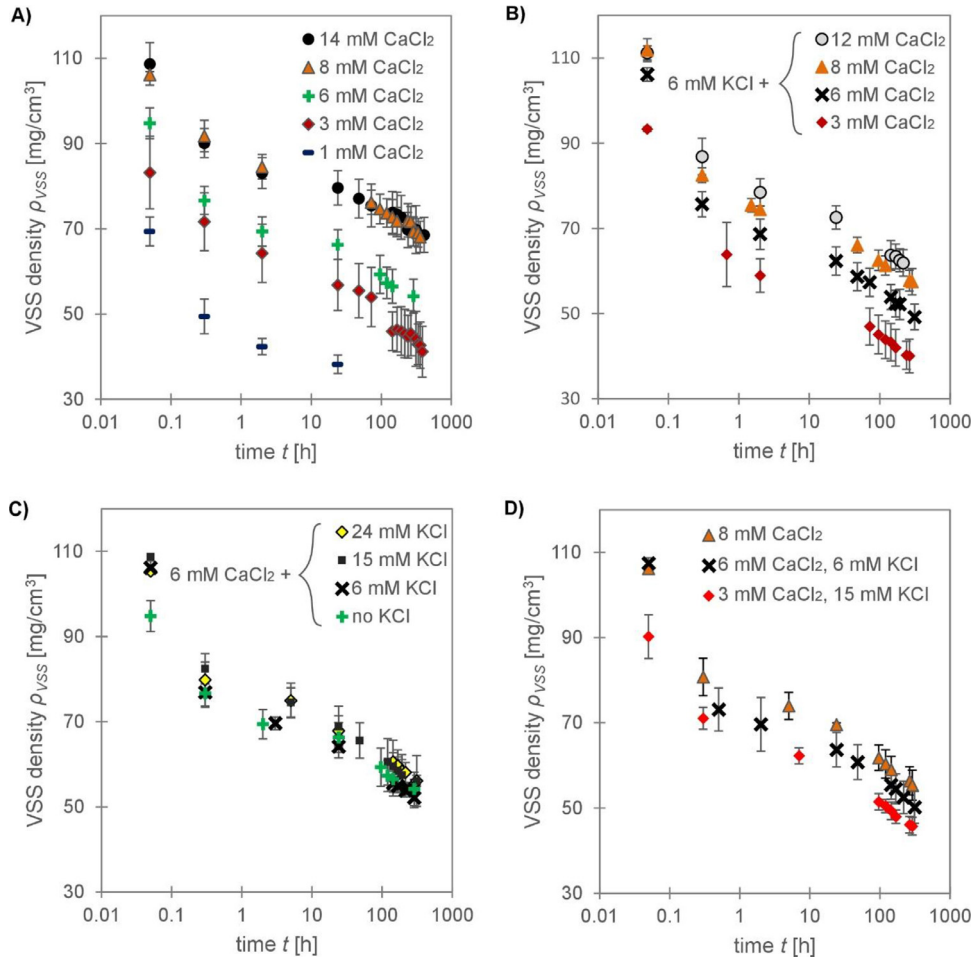

Fig. 4. VSS density ρ_{VSS} as a function of time after formation of ALE gel layers with A) only $CaCl_2$, B) constant KCl, C) constant $CaCl_2$, and D) constant ionic strength. The error bars indicate the standard deviation over 4 samples.

increase. The thickness was converted into VSS density ρ_{VSS}. The development of ρ_{VSS} as a function of time is shown in Fig. 4 for the different ionic compositions.

The density of gel layers with constant $CaCl_2$ and varying KCl concentrations in the supernatant as the only variable showed fairly identical behaviour (Fig. 4C). In contrast, an increase in $CaCl_2$ concentration resulted in higher VSS densities (Fig. 4A, 4B and 4D). An exception from this observation was found at $CaCl_2$ concentrations above 8 mM $CaCl_2$: the density and swelling behaviour did not depend on $CaCl_2$ concentration anymore (Fig. 4A) or only slightly (Fig. 3B), suggesting saturation. Slightly smaller differences in VSS density were observed between the samples with 3 mM, 6 mM and 8 mM $CaCl_2$ shown in Fig. 4D (with varying KCl concentrations) compared to Fig. 4A (without KCl) and 4B (with stable

Table 2
Estimation of osmotic pressure difference [Pa] between the ALE gel layers and the supernatant concentration after 12 days of storage, as calculated by the experimentally determined concentrations of Ca^{2+} and K^+. Errors concern the standard deviation over four samples.

Ca^{2+} [mM]→ K^+ [mM]↓	1	3	6	8	12	14
24	-	-	43.2 ± 25.5	-	-	-
15	-	0.3 ± 1.4	25.0 ± 18.6	-	-	-
6	-	18.4 ± 5.4	47.3 ± 7.1	48.9 ± 6.8	59.1 ± 14.7	-
0	29.3 ± 6.8	23.8 ± 4.0	51.4 ± 6.4	67.2 ± 7.0	-	72.7 ± 14.4

Table 3
Osmotic pressure [Pa] in the ALE gel layers transferred to supernatant with higher $CaCl_2$ concentration. Analysis after 7 days. As a reference, the data for the blank after 12 days is shown as well. Errors concern the standard deviation over four samples, where applicable.

storage time	low blank:3 mM $CaCl_2$ 6 mM KCl	Produced:3 mM $CaCl_2$ 6 mM KCl After 2 days:12 mM $CaCl_2$ 6 mM KCl	Produced:3 mM $CaCl_2$ 6 mM KCl Stored:12 mM $CaCl_2$ 6 mM KCl	high blank:12 mM $CaCl_2$ 6 mM KCl
7 d	33.1	46.6	65.8	-
12 d	18.4 ± 5.4	-	-	59.1 ± 14.7

KCl concentration). The influence of $CaCl_2$ concentration appeared to be much more significant, though.

3.2.2. Ion distribution

Ca^{2+} and K^+ both accumulated in the gel layers (the concentrations are summarised in the SI in Tables A and B). While for Ca^{2+} the concentration found inside the gels initially was up to 25 times that in the supernatant, with a maximum of 4 times the supernatant concentration the accumulation of K^+ inside the gels was much more moderate. As for the VSS densities, a decrease over time was observed.

All types of small ions, provided that they were not irreversibly bound to the gel on the timescale of the experiments, would distribute over the two compartments according to the Donnan potential (cf. section 2.5.1). Whether the ions indeed distributed according to a Donnan equilibrium, was checked by comparing the Donnan potential values calculated from both the distributions of K^+ ions and Ca^{2+} ions (SI, Tables H and J). All values were found between −10 mV and −40 mV, in the range where passively established potentials in biological systems were expected (Sperelakis, 2012). The reasonable agreement between the values calculated from the distributions of Ca^{2+} and K^+ suggests that both types of ions could freely move between the two compartments on the timescale of the experiments.

With Eq. 6 the H^+ activities inside the gel layers were estimated from the Ca^{2+} activities, considering the supernatant H^+ activity was constant at $a_H \approx 10^{-4}$ mM (pH 7). The calculations predict a slight decrease of pH inside the gel layers to pH 6.6 - 6.8.

Based on the Donnan equilibrium and electro-neutrality requirement, the concentration of fixed charges Z in the ALE was estimated using Eq. 4. For the calculations, it was assumed that the contribution of cations other than Ca^{2+} and K^+ to the neutralisation of Z was negligible and that Cl^- (SI, Tables G) was the dominant anion in the system. An average value of 1.05 ± 0.20 mmol/g VSS was obtained (data in SI, Tables K).

3.2.3. Osmotic pressure (network strength)

Because of their very low molar concentrations, the ALE molecules as well as H^+ and OH^- hardly contributed to the osmotic pressure difference and only Ca^{2+}, K^+ and Cl^- were considered. The resulting values for Π, calculated with Eq. 7, are shown in Table 2 and Table 3. After preparation of the gel layers, water flew inside the gel layers to minimise the osmotic pressure difference and caused swelling. At some point, further swelling was prevented by the opposing elastic force of the ALE network. In equilibrium, the osmotic pressure difference is, therefore, an indicator for the network strength. The results show that with increasing $CaCl_2$ concentration in the supernatant, the network strength slightly increased. This indicates that Ca^{2+} was involved in crosslinking of the gel layers.

3.3. Reversibility of swelling by increasing the Ca^{2+} concentration

To differentiate between the influence of $CaCl_2$ available during filtration and $CaCl_2$ available during the swelling, an experiment with a change in $CaCl_2$ concentration during storage was performed. Gel layers were produced with a low calcium concentration (3 mM $CaCl_2$, 6 mM KCl), and then transferred to storage solutions with a high calcium concentration (12 mM $CaCl_2$, 6 mM KCl) directly (sample F) and after two days (sample L). The development of their VSS density in time is shown in Fig. 5, compared to a low blank, prepared and stored with 3 mM $CaCl_2$/6 mM KCl. Also shown is a high blank, produced and stored at 12 mM $CaCl_2$, 6 mM KCl.

Already after 3 minutes, sample F had a higher density than those stored in the low $CaCl_2$ solution (Fig. 5B). The high blank was at this moment still much denser. After 30 min, the density of sample F equalled that of the high blank. In the longer term, it even seemed to reach a slightly higher density than this.

After transferring sample L to a high calcium concentration solution, compaction of the ALE gel layer was observed within a few minutes (Fig. 5C). This process continued for about 6 h. Then an apparent steady-state was reached that lasted for the rest of the observation period (Fig. 5A). The density achieved by this compaction stayed below those of the high blank and sample F. The swelling was, therefore, described as partly reversible. Similarly, the Ca^{2+} content per VSS in the transferred gel layers did not completely reach that of the high blank (data not shown).

In accordance with the density data, the osmotic pressure data for the reversibility experiment (Table 3) showed a clear hierarchy in network strength increasing from the low blank via the one transferred to 12 mM $CaCl_2$ after 2 days to the one directly stored in 12 mM $CaCl_2$. Also in this case, what happened during the two days of storage in the low concentration solution, was partly irreversible.

3.4. Additional ripening

The experiments described in section 3.2 were limited to 12 days because that was found to be the period over which all gel layers kept their macroscopic integrity, which was a requirement to calculate and compare the densities. When stored for a more

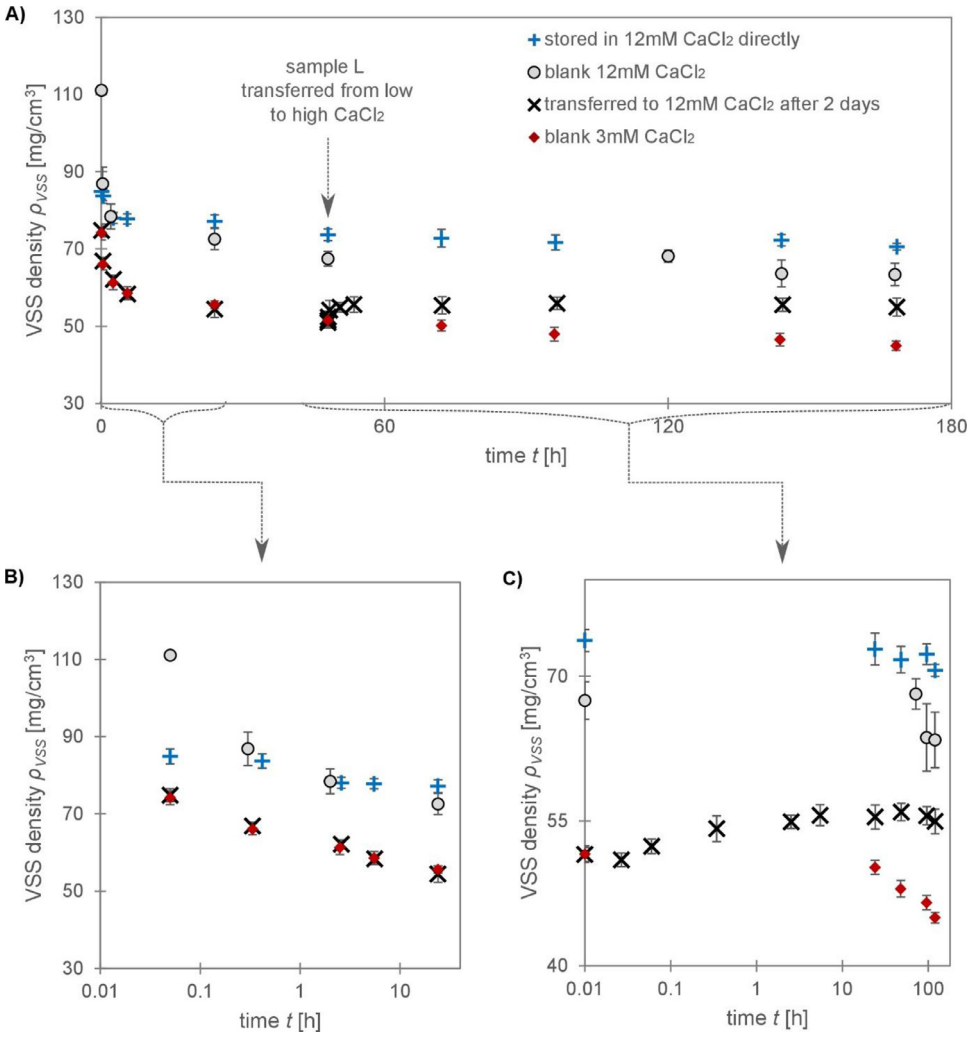

Fig. 5. Comparison of the swelling behaviour of gel layers produced with 3 mM CaCl2 and 6 mM KCl and subsequently stored in 12 mM CaCl2/6 mM KCl (high calcium, sample F, +) and 3 mM CaCl2/6 mM KCl for two days and then transferred to 12 mM CaCl2/6 mM KCl (low calcium, sample L, x). For comparison, blanks produced and stored with either high (circle) or low (diamond) calcium concentration are shown. A) shows the whole range of the experiment, B) zoomed in on the first two days and C) zoomed in on the swelling after transfer to the higher calcium concentration after two days. Since those were single experiments, the error bars show the standard deviation over 4 samples only for the high blank.

extended period, or with less optimised concentrations of ALE and ions, initially voids were observed in the gel layers. Eventually, a fibrous network developed. This development is illustrated by the optical coherence tomography (OCT) pictures in Fig. 6 for gel layers produced with 60 mg/L ALE and 45 mM ionic strength 30 min after production, after 3 days and after 5 days.

The used OCT system had a resolution in the range of 10 µm, meaning that pores could only be detected as soon as they reached this size in both dimensions. It seems likely that these pores developed on a micro-scale before structural changes could be observed with the OCT. Structural rearrangements in the ALE network were considered the major cause for the observed slow swelling of the gel layers described in sections 3.1-3.3. Increasing the resolution, for example, by taking SEM pictures on stabilised samples, may reveal such changes on the microstructure level.

4. Discussion

The gel layers' composition and appearance result from the balances between electrostatic interactions in the gel, osmotic pressure differences between the gel and the outside solution, and the ability of the gel network to withstand swelling by water intake. These mechanisms are discussed below.

4.1. Ion distribution

While the high specificity and chelating nature of the Ca^{2+} crosslinks in alginate are well known, the present results indicate no specific (irreversible) binding of Ca^{2+} to ALE. Therefore, it is expected that Ca^{2+} can be easily removed, for example, by dilution, or replaced by other ions. Based on this study's results, other divalent cations are probably also able to induce the crosslinking. Formation of stable gels with comparable elastic properties has indeed been confirmed with a whole range of divalent cations (Felz et al., 2020a). To identify the (non)specificity of those interactions, composition analysis like done in this study can be used. The difference with alginate in binding may be explained by the finding that a significant amount of the charged groups in ALE is sulfate rather than carboxylate (Felz et al., 2020b).

Based on electro-neutrality and the Donnan potential, the number of negative charges in the ALE was calculated as 1.05 ± 0.20 mmol/g VSS. One Ca^{2+} cation could neutralise two negative charges in theory, so this value is well in line with the measured Ca^{2+} concentrations in the ALE gel layers of 200 - 700 μmol per g VSS (SI, Fig. A). It should be noted, however, that following the Donnan potential also Cl^- distributed over gel layer and super-

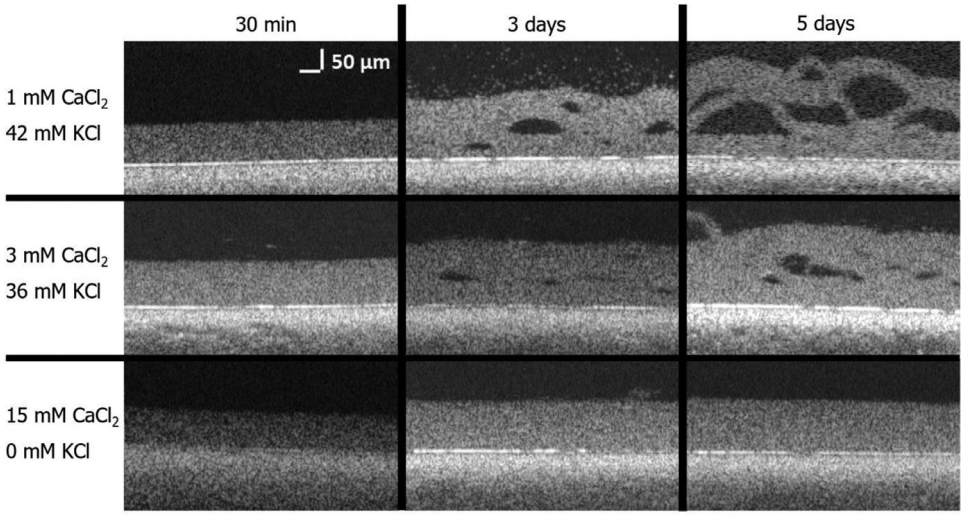

Fig. 6. Ripening of ALE gel layers observed by OCT over 5 days. The images show an ALE gel made from a solution of 60 mg/L ALE and 45 mM ionic strength. Note the changed composition in comparison with the measurements described earlier, which accelerated the ripening process.

natant. As a consequence, not every Ca^{2+} ion inside the gel layers contributed to the crosslinking.

The pK_a values of the carboxylate groups of mannuronic and guluronic acid were found at 3.38 and 3.65 (Draget et al., 1994). These groups are all negatively charged at pH 7 and thus contributed to Z in the ALE gel layers. Sulfates are strong acids, so negatively charged independently of pH. Therefore, the current experiments and calculations did not identify what groups of ALE were involved in crosslinking. On the basis of further chemical characterisation of ALE, experiments in which the pH is varied can be useful for deeper insight.

4.1.1. Correlation between Ca^{2+} content, density and strength of the ALE gel layers

With increasing $CaCl_2$ concentration in the supernatant, the ALE gel layers as prepared in this work were found denser until a plateau was reached around 8 mM Ca^{2+} (Fig. 4). Such correlation has been studied intensively for alginate gels (Davidovich-Pinhas and Bianco-Peled, 2010) and has been explained with a higher number of crosslinks with increasing Ca^{2+} concentration. Also for bacterial EPS, Ca^{2+} availability has been directly linked to denser films (Goode and Allen, 2011; Körstgens et al., 2001).

This work shows, in addition, a correlation between Ca^{2+} content and density and the network strength (cf. section 3.2.3). The supernatant's ionic composition defined the ion concentration inside the gels (given the fixed amount of charges of the ALE per g VSS) and thus the osmotic pressure difference (section 2.5). At the same time, the network strength determined the maximum amount of water that could be taken up to reduce the osmotic pressure difference. Apparently, over time this maximum amount increased, associated with a slow but irreversible weakening of the network structure (as shown in Table 3, further discussion of the reversibility in section 4.3). The mechanisms behind this effect are probably related to the slow structural rearrangement resulting in void formation (Fig. 6) and require further investigation.

4.2. Hydraulic resistance of ALE gel layers

A positive correlation between EPS density and hydraulic resistance of biofilms has been postulated before (Desmond et al., 2018; Jafari et al., 2018). Also, the Ca^{2+} concentration in ALE films has been correlated to flux decline in membrane filtration (Herzberg et al., 2009). This goes along with the finding that the specific cake layer resistance of the ALE gel layers in this work slightly increased with supernatant $CaCl_2$ concentration (Fig. 3). In this context, it attracted attention that while the VSS density reached a maximum around 110 mg/cm^3, the specific resistance still slightly increased (e.g. between 8 mM $CaCl_2$ and 14 mM $CaCl_2$, Fig. 3). The differences in relation to the standard deviations (cf. SI, Table E) were so small, however, that no further conclusions could be drawn from these data.

4.3. Compressibility, relaxation and ripening

Compressibility, as observed for the ALE gel layers in this work, is a feature of biofilms that has been investigated for several years (Jafari et al., 2018), and that has also been used as an indication for the viscoelastic behaviour of biofilms (Safari et al., 2015). The relaxation of biofilms after compression has been described with the help of Maxwell springs (Jones et al., 2011; Safari et al., 2015), as an approximately exponential process. In our experiments, relaxation was expected as soon as the filtration pressure was released. Due to experimental restrictions, the changes in the thickness of the ALE gel layers in this study were only recorded from ca. 3 minutes after pressure release. Therefore, a quantitative analysis of the collected data appeared unreliable. For accurate collection and analysis of relaxation data to extract characteristic viscoelastic data, systems with controllable compression and instantaneous observation of the stress and strain are needed. Such experiments will also be of interest to distinguish between cross-linked gel layers and non-cross-linked cake layers. Also, the influence of different gel production procedures could be interesting in this regard.

Interesting observations in this study were the long continuation of the swelling (Fig. 4), and the eventual development of a fibre-like ALE network (Fig. 6). Fibrous structures have been observed in biofilm matrices (Romero et al., 2010) and are usually attributed to amyloids. The present study suggests that ALE also forms such fibres, in accordance with previous work (Lin et al., 2018). The observation that the swelling process was only partly reversible (section 3.3) indicates that a slow molecular rearrangement started with the initial formation of microscopic voids in the structure (cf. Jafari et al., 2018) right when the pressure was released. Because the network had started to be weakened by the voids (cf. Table 3, section 4.1.1), neither the density nor the osmotic pressure difference of gel layers directly stored in the higher $CaCl_2$ concentration could be reached by later transferred samples. Fi-

brous structures and a decrease in density over longer time scales (between 7 and 12 days) were especially found in the gel layers that were prepared with and stored at the lower $CaCl_2$ concentrations (1 and 3 mM). Apparently, fibre formation was prevented or delayed by Ca^{2+} crosslinks in the network.

According to Desmond et al. (Desmond et al., 2018b), compression caused by filtration pressure is reversible for structurally homogeneous biofilms and irreversible for films with a heterogeneous structure. This work supports this finding, showing that networks with voids were weaker than more homogenous networks without voids.

4.4. Outlook

This work provides valuable insight into the interaction between ALE and Ca^{2+} in the presence of K^+ and Cl^-. As a next step, the influence of Ca^{2+} content of ALE gels on their mechanical properties such as modulus, strength and adhesion will be investigated. While a closer look on the swelling behaviour can be a start, e.g. by observation in the filtration cell during filtration, possibly also under application of different pressures, determining the gels' viscoelastic properties by rheological measurements will provide quantitative data. This will make it possible to link the composition to mechanical properties of the gel layers and will be the subject of a forthcoming paper.

The system of ALE and specific ions still represents a simplified model for the EPS matrix of biofilms. The model can be extended by adding other kinds of molecules, such as peptides, humic acids and eDNA, to eventually get close to real biofilms' complexity. Evaluating the interactions within the ALE network, also beyond electrostatic ones, with added compounds, and based on a better chemical characterisation of ALE and EPS can lead the path towards understanding the cohesive forces of biofilms. This is an important step towards tailored cleaning strategies.

5. Conclusions

- The density and network strength of ALE gel layers depend on crosslinking with a multivalent cation like Ca^{2+}.
- Ca-ALE gel layers produced on a membrane by dead-end filtration swell, after pressure release, for up to 12 days. This process is accompanied by a weakening of the structure and is partially irreversible. One of the mechanisms behind it is a slow molecular rearrangement of ALE, culminating in the development of a fibrous structure.
- The accumulation of cations, including Ca^{2+}, over a Ca-ALE gel and its supernatant, can be described as a result of a Donnan potential induced by the fixed charges on the extracellular polymers. This indicates that no specific binding is involved in the physical crosslinking of ALE gel layers by Ca^{2+}.

Declaration of Competing Interest

The authors declare that they have no known competing financial interests or personal relationships that could have appeared to influence the work reported in this paper.

Acknowledgement

This work was performed in the cooperation framework of Wetsus, European Centre Of Excellence For Sustainable Water Technology (www.wetsus.nl). Wetsus is funded by the Dutch Ministry of Economic Affairs and Ministry of Infrastructure and Environment, the European Union Regional Development Fund, the Province of Fryslân, and the Northern Netherlands Provinces. The authors would like to thank the members of the research theme "Biofilms" for fruitful discussions and financial support.

Supplementary materials

Supplementary material associated with this article can be found, in the online version, at doi:10.1016/j.watres.2021.116959.

References

Bajpai, S.K., 2001. Swelling studies on hydrogel networks - a review. J. Sci. Ind. Res. (India). 60, 451–462.
Davidovich-Pinhas, M., Bianco-Peled, H., 2010. A quantitative analysis of alginate swelling. Carbohydr. Polym. 79, 1020–1027. doi:10.1016/J.CARBPOL.2009.10.036.
Desmond, P., Morgenroth, E., Derlon, N., 2018. Physical structure determines compression of membrane biofilms during Gravity Driven Membrane (GDM) ultrafiltration. Water Res. 143, 539–549. doi:10.1016/j.watres.2018.07.008.
Draget, K.I., Skjåk Bræk, G., Smidsrød, O., 1994. Alginic acid gels: the effect of alginate chemical composition and molecular weight. Carbohydr. Polym. 25, 31–38. doi:10.1016/0144-8617(94)90159-7.
Felz, S., Al-Zuhairy, S., Aarstad, O.A., van Loosdrecht, M.C.M., Lin, Y.M., 2016. Extraction of Structural Extracellular Polymeric Substances from Aerobic Granular Sludge. J. Vis. Exp. e54534. doi:10.3791/54534.
Felz, S., Kleikamp, H., Zlopasa, J., van Loosdrecht, M.C.M., Lin, Y., 2020a. Impact of metal ions on structural EPS hydrogels from aerobic granular sludge. Biofilm 2. doi:10.1016/j.bioflm.2019.100011.
Felz, S., Neu, T.R., van Loosdrecht, M.C.M., Lin, Y., 2020b. Aerobic granular sludge contains Hyaluronic acid-like and sulfated glycosaminoglycans-like polymers. Water Res 169. doi:10.1016/j.watres.2019.115291.
Flemming, H.-C., 2020. Biofouling and me: My Stockholm syndrome with biofilms. Water Res. 173, 115576. doi:10.1016/j.watres.2020.115576.
Ganji, F., Vasheghani-Farahani, S., Vasheghani-Farahani, E., 2010. Theoretical description of hydrogel swelling: a review. Irymer Journalanian Pol. 19, 375–398. doi:10.1007/s12303-009-0004-6.
Goode, C., Allen, D.G., 2011. Effect of calcium on moving-bed biofilm reactor biofilms. Water Environ. Res. 83, 220–232 10.2175/106143010×12780288628255.
Hamer, W.J., Wu, Y.-C., 1972. Osmotic coefficients and mean activity coefficients of uni-univalent electrolytes in water at 25°C. J. Phys. Chem. Ref. Data 1, 1047–1100. doi:10.1063/1.3253108.
Herzberg, M., Kang, S., Elimelech, M., 2009. Role of Extracellular Polymeric Substances (EPS) in biofouling of reverse osmosis membranes. Environ. Sci. Technol. 43, 4393–4398. doi:10.1021/es900087j.
Jafari, M., Desmond, P., van Loosdrecht, M.C.M., Derlon, N., Morgenroth, E., Picioreanu, C., 2018. Effect of biofilm structural deformation on hydraulic resistance during ultrafiltration: a numerical and experimental study. Water Res 145, 375–387. doi:10.1016/j.watres.2018.08.036.
Jones, W.L., Sutton, M.P., McKittrick, L., Stewart, P.S., 2011. Chemical and antimicrobial treatments change the viscoelastic properties of bacterial biofilms. Biofouling 27, 207–215. doi:10.1080/08927014.2011.554977.
Kielland, J., 1937. Individual activity coefficients of ions in aqueous solutions. J. Am. Chem. Soc. 59, 1675–1678. doi:10.1021/ja01288a032.
Körstgens, V., Flemming, H.-C., Wingender, J., Borchard, W., 2001. Influence of calcium ions on the mechanical properties of a model biofilm of mucoid Pseudomonas aeruginosa. Water Sci. Technol. 43, 49–57. doi:10.1371/journal.pone.0091935.
Li, Q., Elimelech, M., 2004. Organic fouling and chemical cleaning of nanofiltration membranes: measurements and mechanisms. Environ. Sci. Technol. 38, 4683–4693. doi:10.1021/es0354162.
Lin, Y.M., de Kreuk, M., van Loosdrecht, M.C.M., Adin, A., 2010. Characterization of alginate-like exopolysaccharides isolated from aerobic granular sludge in pilot-plant. Water Res 44, 3355–3364. doi:10.1016/j.watres.2010.03.019.
Lin, Y.M., Reino, C., Carrera, J., Pérez, J., van Loosdrecht, M.C.M., 2018. Glycosylated amyloid-like proteins in the structural extracellular polymers of aerobic granular sludge enriched with ammonium-oxidizing bacteria. Microbiologyopen 7. doi:10.1002/mbo3.616.
Listiarini, K., Sun, D.D., Leckie, J.O., 2009. Organic fouling of nanofiltration membranes: Evaluating the effects of humic acid, calcium, alum coagulant and their combinations on the specific cake resistance. J. Memb. Sci. 332, 56–62. doi:10.1016/j.memsci.2009.01.037.
Nagashima, A., 1977. Viscosity of water substance—new international formulation and its background. J. Phys. Chem. Ref. Data 6, 1133–1166. doi:10.1063/1.555562.
Pronk, M., de Kreuk, M.K., de Bruin, B., Kamminga, P., Kleerebezem, R., van Loosdrecht, M.C.M., 2015. Full scale performance of the aerobic granular sludge process for sewage treatment. Water Res 84, 207–217. doi:10.1016/j.watres.2015.07.011.
Radchenkova, N., Boyadzhieva, I., Atanasova, N., Poli, A., Finore, I., Di Donato, P., Nicolaus, B., Panchev, I., Kuncheva, M., Kambourova, M., 2018. Extracellular polymer substance synthesized by a halophilic bacterium Chromohalobacter canadensis 28. Appl. Microbiol. Biotechnol. 102, 4937–4949. doi:10.1007/s00253-018-8901-0.
Romero, D., Aguilar, C., Losick, R., Kolter, R., 2010. Amyloid fibers provide structural integrity to Bacillus subtilis biofilms. Proc. Natl. Acad. Sci. 107, 2230–2234. doi:10.1073/pnas.0910560107.
Roorda, J.H., van Loosdrecht, M.C.M., 2001. New parameter for monitoring fouling during ultrafiltration of WWTP effluent. Water Sci. Technol. 43, 241–248. doi:10.2166/wst.2001.0631.

Safari, A., Tukovic, Z., Walter, M., Casey, E., Ivankovic, A., 2015. Mechanical properties of a mature biofilm from a wastewater system: from microscale to macroscale level. Biofouling 31, 651–664. doi:10.1080/08927014.2015.1075981.

Seviour, T., Derlon, N., Dueholm, M.S., Flemming, H.C., Girbal-Neuhauser, E., Horn, H., Kjelleberg, S., van Loosdrecht, M.C.M., Lotti, T., Malpei, M.F., Nerenberg, R., Neu, T.R., Paul, E., Yu, H., Lin, Y., 2019. Extracellular polymeric substances of biofilms: Suffering from an identity crisis. Water Res. 151, 1–7. doi:10.1016/j.watres.2018.11.020.

Seviour, T., Pijuan, M., Nicholson, T., Keller, J., Yuan, Z., 2009. Understanding the properties of aerobic sludge granules as hydrogels. Biotechnol. Bioeng. 102, 1483–1493. doi:10.1002/bit.22164.

Sperelakis, N., 2012. Chapter 10 - Gibbs-donnan equilibrium potentials. In: Cell Physiology Source Book. Elsevier BV, pp. 147–151. doi:10.1016/B978-0-12-387738-3.00010-X.

van den Brink, P., Zwijnenburg, A., Smith, G., Temmink, H., van Loosdrecht, M., 2009. Effect of free calcium concentration and ionic strength on alginate fouling in cross-flow membrane filtration. J. Memb. Sci. 345, 207–216. doi:10.1016/j.memsci.2009.08.046.

Wang, X., Spencer, H.G., 1998. Calcium alginate gels: formation and stability in the presence of an inert electrolyte. Polymer (Guildf) 39, 2759–2764. doi:10.1016/S0032-3861(97)00597-1.